Uncertainty Analysis Methodology for Measurements of Dynamic Millimeter-Wave Channels

ROBBERT SCHULPEN[ID], A. BART SMOLDERS (Senior Member, IEEE),
ULF JOHANNSEN[ID] (Senior Member, IEEE), AND L. A. BRONCKERS[ID] (Member, IEEE)

Department of Electrical Engineering, Eindhoven University of Technology, 5600 MB Eindhoven, The Netherlands

CORRESPONDING AUTHOR: R. SCHULPEN (e-mail: r.schulpen@tue.nl)

ABSTRACT Quantification of uncertainties in the results of channel sounding measurements is important for their interpretation and further usage. In this paper, a novel uncertainty analysis methodology to quantify uncertainties of condensed parameters in measurements of dynamic millimeter-wave channels is presented. The bandwidth limitation and multipath threshold are identified as important impairments. Therefore, the methodology provides three uncertainty metrics for condensed parameters, namely a standard uncertainty to quantify the impact of random variations; a bias due to the multipath threshold; and a total bias including the impact of the bandwidth limitation. These uncertainty metrics are highly channel dependent. Therefore, the proposed methodology creates reference channels, which are representative of corresponding measured channels. Hardware and processing impairments are included in the analysis via a Monte Carlo simulation. This results in a general methodology that can quantify uncertainties in both static and dynamic channel measurements of any wideband channel sounder. The methodology is implemented, verified and demonstrated for the TU/e channel sounder, which exemplifies how it can be used. The proposed methodology can improve the analysis, interpretation and reporting of channel measurement results.

INDEX TERMS Channel dynamics, channel sounding, delay spread, Doppler spread, millimeter-wave propagation, path loss, uncertainty analysis.

I. INTRODUCTION

THE MILLIMETER-WAVE (mm-wave) band is adopted in 5G to enable ultra-high data-rate and high capacity applications. The use of mm-waves in cellular communication requires new channel models to account for the significantly different propagation conditions compared to sub-6 GHz communication [1], [2]. The small wavelengths at mm-waves limit diffraction [3] and hence increase shadowing and blockage probability, making channel dynamics of particular interest for mm-wave channels. Several institutions around the world have developed mm-wave channel sounders (e.g., [4], [5], [6], [7], [8], [9]), which are needed for the development and verification of channel models. The high cost and complexity of mm-wave channel sounders often requires trade-offs between measurable parameters, measurement time and resolution. The TU/e channel sounder,

described in [10], is designed to characterize dynamic mm-wave channels because of the increased importance of channel dynamics at mm-waves.

Verification of mm-wave channel sounders is important to ensure accurate channel measurement results and has recently gained special interest of the channel sounding community in the 5G Millimeter-Wave Channel Model Alliance [11] and the IEEE P2982 working group on "Recommended Practice for Mm-Wave Channel Sounder Verification" [12]. Channel sounder descriptions in literature often include a verification using wired back-to-back measurements [7], [13], wired artifacts [14], [15] or wireless line-of-sight (LOS) measurements [5], [8] to show that results comply to expected behavior. Recently, research has been reported on channel sounding errors in multipath-component (MPC) characteristics and channel
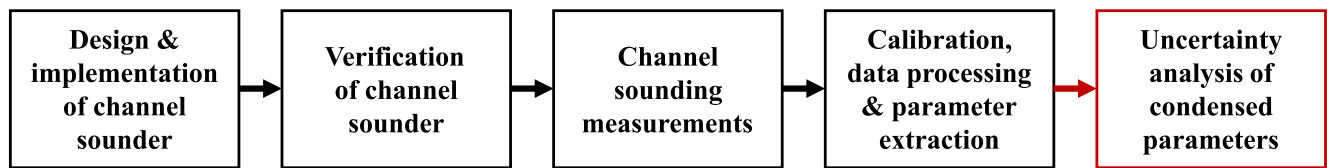
FIGURE 1. Block diagram illustrating the workflow for mm-wave channel sounding measurements. The proposed uncertainty analysis of the extracted condensed parameters follows after the channel measurements and processing as a final stage.

metrics [2], [16]. In [16], a quantitative comparison between the measurement results of a channel sounder and a vector network analyzer (VNA) as reference is made for three channels. In contrast, a cross-validation of multiple channel sounders is performed in [2] by deriving measurement errors with respect to 20 "ground-truth" reference channels that are obtained from a quasi-deterministic channel model. These channel sounder verification practices are important for the correction and prevention of errors in channel sounding measurements, but they do not quantify the uncertainties in these measurements.

Therefore, a methodology for uncertainty estimation is needed to obtain quantitative bounds on the results of channel sounding measurements. In this paper, we introduce a generally applicable uncertainty estimation methodology for wideband channel sounding. The outputs of this methodology are uncertainty metrics, which quantify the uncertainties in extracted parameters of channel sounding measurements. Examples of extracted parameters are path loss, rms delay spread, rms Doppler spread (we omit the designation rms in the remaining of this paper), angle-of-departure and angle-of-arrival, which are jointly referred to as condensed parameters [17]. The typical workflow for mm-wave channel sounding is depicted Fig. 1, where the uncertainty analysis is added as final stage. In contrast to the verification of a channel sounder, the uncertainty analysis needs to be performed after the channel sounding measurements and processing. This is due to the high channel dependency of the uncertainties, which is illustrated in Section II.

In this paper, we address four key challenges to enable uncertainty estimation of channel sounding measurements:

1) The ambiguity in the definition of the reference channel. Different channel definitions result in different uncertainty estimates.
2) The high channel dependency of the uncertainties. Uncertainties are channel-specific and need to be estimated for individual channel measurements.
3) The impact of channel dynamics on the uncertainties. The methodology should account for dynamic effects in channel measurements.
4) The reconstruction of interference in a reference channel. Interference effects due to the bandwidth limitation of a measurement can increase the uncertainties and should be accounted for.

The proposed uncertainty analysis methodology is of a general nature and could be applied to both static and dynamic measurements of any wideband channel sounder. The methodology is implemented for and verified with dynamic measurements of the TU/e channel sounder, and the ensuing results for the uncertainty metrics are presented and discussed.

The remainder of this paper is organized as follows. An overview of the proposed uncertainty analysis methodology is described in Section II. To illustrate this methodology, it is implemented for the TU/e channel sounder in Section III. Using this implementation, the methodology is verified in Section IV. Uncertainty metrics for measurements of the TU/e channel sounder are presented in Section V. This work is concluded in Section VI.

II. UNCERTAINTY ANALYSIS METHODOLOGY

The "guide to the expression of uncertainty in measurement" defines "uncertainty of measurement" as doubt about the validity of the result of a measurement [18]. The results of a channel sounding measurement or campaign are typically the condensed parameters, which are reported quantitatively and used to draw qualitative conclusions. The proposed uncertainty analysis methodology estimates uncertainty metrics for these parameter.

The relevant aspects of the methodology are discussed below. In Section II-A, the impairments in channel sounding measurements are described. The definition and selection of reference channels is discussed in Section II-B. Using these definitions, uncertainty metrics are defined in Section II-C. Finally, an overview of the resulting uncertainty analysis methodology is presented in Section II-D.

A. IMPAIRMENTS IN CHANNEL SOUNDING MEASUREMENTS

Impairments are phenomena that can increase the uncertainty in channel sounding measurements. In this paper, these impairments are divided into two categories: 1) hardware impairments; and 2) processing impairments.

1) HARDWARE IMPAIRMENTS

Hardware impairments can be caused by hardware imperfections, hardware limitations and dependencies of the hardware on environmental effects like temperature. Examples of hardware impairments are thermal noise, quantization noise,
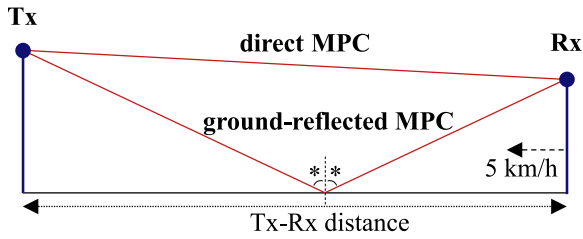
FIGURE 2. Side view of two-ray ground-reflection model with a dynamic receiver (Rx) moving towards the transmitter (Tx).
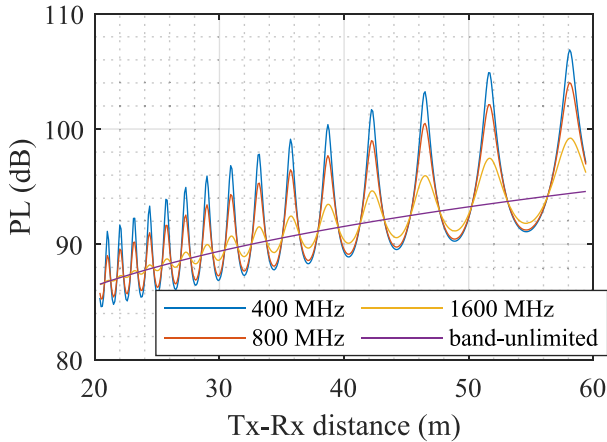

FIGURE 3. Band-limited (400 MHz, 800 MHz and 1600 MHz) and band-unlimited path loss for two-ray ground-reflection model. The bandwidth limitation causes interference between the direct and ground-reflected MPCs, which results in a ripple on the band-limited responses.

FIGURE 4. Average PDP peak and corresponding PDP peaks of the individual snapshots of a measurement along the two-ray ground-reflection model track. The interference between the direct MPC and ground-reflected MPC causes magnitude variations between the PDP peaks of the individual snapshots.

clock jitter and drift, amplifier non-linearity, antenna pattern ambiguities, thermal dependencies of RF equipment and the bandwidth limitation of the channel sounder. The estimation of thermal noise, quantization noise and clock jitter is discussed in Section III-C. The bandwidth limitation is discussed in more detail below.

The inherent bandwidth limitation of a channel sounder can highly increase the uncertainty in a measurement result. The finite bandwidth limits the resolution at which MPCs can be distinguished. MPCs that cannot be distinguished from each other interfere and introduce a bias in the measurement result. Channel sounders typically use wideband signals to minimize this effect, but this bias can remain significant in wideband channel sounding as will be shown using the two-ray ground-reflection model illustrated in Fig. 2. In this model, the receiver (Rx) moves at 5 km/h towards the transmitter (Tx) over a concrete floor in the presence of a direct and ground-reflected MPC. The heights of the Tx and Rx are 1.8 m and 1.5 m, respectively. The reflection coefficient of the concrete floor is estimated using the properties of concrete given in [19]. The path loss can then be calculated from the amplitudes of the direct MPC and ground-reflection MPC. Fig. 3 depicts the path loss for various bandwidths for a Tx-Rx distance between 20 m and 60 m. The band-unlimited response shows the path loss in case of no bandwidth limitation and follows the inverse-square law as function of distance
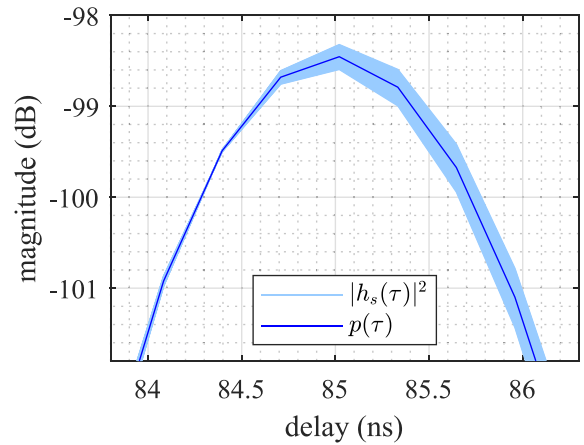
for both MPCs. In case of the band-limited observations (400 MHz, 800 MHz and 1600 MHz), the two MPCs cannot be fully distinguished and the resulting interference causes a ripple on the path loss. Thus, the band-limited responses in Fig. 3 introduce a bias with respect to the band-unlimited response, which could be regarded as a component of the combined uncertainty (this will be addressed in Section II-C).

The bandwidth limitation also introduces an effect that is specific to dynamic measurements, which contain MPCs with non-zero Doppler frequencies. A channel sounding measurement typically consists of multiple snapshots to enable averaging, Doppler spread estimation or angle-of-arrival estimation. In a dynamic measurement, increased differences between the channel impulse responses (CIRs) of these snapshots occur when multiple MPCs interfere. This effect is illustrated in Fig. 4 for a measurement along the track in Fig. 2, where $|h_s(\tau)|^2$ is the power delay profile (PDP) of snapshot s and $p(\tau)$ is the average PDP, which is calculated as

$$p(\tau) = \frac{1}{N_s} \sum_{s=1}^{N_s} |h_s(\tau)|^2, \tag{1}$$

where N_s is the number of snapshots and τ is the delay. The PDPs are obtained using a 400 MHz bandwidth and 50 snapshots, which are recorded at a trigger rate f_t of 4.88 kHz (these settings are obtained from the TU/e channel sounder implementation, which is explained in the Appendix). In contrast to Fig. 3, Fig. 4 shows variations within a measurement of $p(\tau)$ instead of variations between different measurements. The interference between the two MPCs in this channel is different for each snapshot, which causes differences between the PDPs of these snapshots. These variations increase the uncertainty in condensed parameters that are derived from the average PDP. Moreover, the impact of this effect increases for higher Doppler frequencies (larger
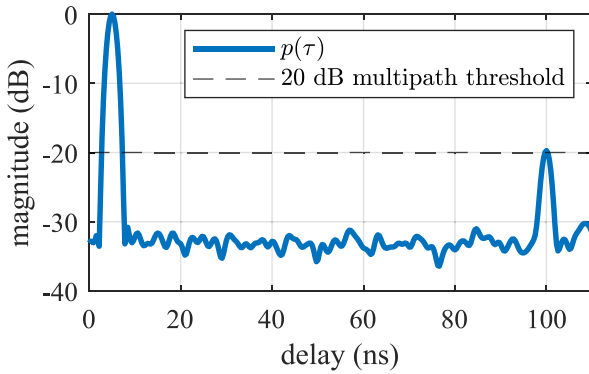
FIGURE 5. Example of how the multipath threshold of the PDP introduces a non-linear effect, which affects the uncertainty in a condensed parameter. The second MPC can appear just above or below the multipath threshold due to random impairments. The resulting delay spread increases to 5 ns when this MPC is above the threshold, which leads to a large uncertainty in delay spread.

variations in the PDP peaks) and smaller N_s (less averaging). Therefore, this phenomenon should be accounted for in the uncertainty analysis.

2) PROCESSING IMPAIRMENTS

Processing impairments are introduced in the processing of digitized measurement data. The channel sounder calibration is applied in the data processing step in order to remove the response of the channel sounder itself from the measurement data. Imperfections of the calibration can introduce spurious MPCs and a bias in the true MPCs, which can affect the extracted condensed parameters. Another inevitable processing impairment is the use of a threshold to distinguish true MPCs from spurious MPCs. Spurious MPCs could occur due to thermal noise and limitations of the calibration. The threshold can be defined with respect to either the noise floor [20] or the strongest MPC in the PDP [16]. We use the second definition in this paper and refer to this threshold as the multipath threshold. This multipath threshold can introduce an error and increase the uncertainties of condensed parameters by excluding weak (true) MPCs. A simple example of this is illustrated in Fig. 5. Random impairments affect the magnitude of the second MPC at 100 ns such that this MPC occurs either above or below the 20 dB multipath threshold. If this MPC is above the multipath threshold, then the delay spread will be 5 ns larger than if it is below the multipath threshold. This highly increases the uncertainty in delay spread.

B. DEFINITION AND SELECTION OF REFERENCE CHANNELS

Section II-A introduced the bandwidth limitation and multipath threshold as possible impairments. These aspects could instead be regarded as being part of the channel itself, meaning that they do not contribute to the uncertainty of a channel sounding measurement. This raises the question of how to define the reference channel. In [16], the reference is a band-limited channel measurement by a

VNA, where a multipath threshold is applied to the measurement. In contrast, the reference channel in [2] does not contain a bandwidth limitation or multipath threshold. The 'best' channel definition depends on the purpose or intended application of the channel sounding results. Thus, in this paper, we introduce three channel definitions to make our proposed uncertainty analysis methodology widely applicable for various types of channel sounding measurements:

1) *Thresholdless band-unlimited channel:* A channel in which each MPC is represented by a Dirac delta pulse with individual MPC characteristics. This definition treats the bandwidth limitation, multipath threshold and other hardware and processing impairments (e.g., noise and calibration) as measurement impairments. It is a rather fundamental definition of the channel and gives its most general description. However, this channel cannot be measured directly, because a channel sounder is always band-limited. This channel could be approximated if the resolutions of the channel sounder are sufficient to be able to distinguish all characteristics of the individual MPCs. Fig. 3 shows that this is not always achievable in practice using typical measurement bandwidths.

2) *Thresholdless band-limited channel:* A channel representation that includes a bandwidth limitation, but no multipath threshold. In this definition, the bandwidth limitation of the channel sounder is treated as part of the channel itself. The multipath threshold and other hardware and processing impairments are regarded as measurement impairments. This channel definition can be approximated by channel sounding measurements if the multipath threshold value is high enough to include all MPCs that significantly affect the condensed parameters.

3) *Thresholded band-limited channel:* A channel definition for which the bandwidth limitation and multipath threshold are regarded as part of the channel. Therefore, only other hardware and processing impairments contribute to the uncertainty in a measurement using this channel definition. This definition is especially useful for channel measurements for a specific use case with a known bandwidth and instantaneous dynamic range.

The uncertainty metrics that will be introduced in Section II-C are related to these channel definitions.

Besides the definition of the reference channel, the selection of reference channels is also important. For example, the theoretical example in Fig. 5 shows that even a weak MPC in a LOS channel could largely increase the uncertainty in delay spread, which is also found in actual channel sounding measurements as is shown in Fig. 7 in [10]. This shows that the uncertainty in the measured condensed parameters can be highly channel dependent. Therefore, the reference channels in the proposed methodology are based on the measured channels from which the uncertainties are desired. This

TABLE 1. Uncertainty metrics for the different channel definitions.

Channel definition	Applicable uncertainty metrics
Thresholdless band-unlimited channel	ϵ_c^{CP} and σ_c^{CP}
Thresholdless band-limited channel	$\epsilon_c^{\mathrm{TH,CP}}$ and σ_c^{CP}
Thresholded band-limited channel	σ_c^{CP}

ensures that the reference channels are representative of the measured channels. This, in turn, makes the estimated uncertainties also representative of the uncertainties in the channel measurements.

C. UNCERTAINTY METRICS

Uncertainty metrics are derived for the condensed parameters of every reference channel c individually. Three uncertainty metrics are defined:

1) σ_c^{CP}: A standard uncertainty, which is a measure for the uncertainty due to random variations in a condensed parameter. σ_c^{CP} is the combined standard uncertainty in case of the thresholded band-limited channel definition.

2) $\epsilon_c^{\mathrm{TH,CP}}$: The bias between the condensed parameter of a thresholded and thresholdless band-limited channel. This parameter provides the bias that is introduced by the use of a multipath threshold.

3) ϵ_c^{CP}: The bias between the condensed parameter of a thresholded band-limited and thresholdless band-unlimited channel. This metric indicates the total bias in a measured condensed parameter with respect to its thresholdless band-unlimited equivalent. It quantifies the effects of the multipath threshold and bandwidth limitation.

Table 1 summarizes the relevant metrics for each channel definition from Section II-B. The impact of the bandwidth limitation and multipath threshold are quantified by a bias, because these impairments result in a constant offset for a given reference channel. In combination with random impairments, the bandwidth limitation and multipath threshold can also amplify random variations as is exemplified in Fig. 5. This effect is captured by σ_c^{CP} for each of the channel definitions.

The uncertainty metrics above are defined for classical parameter extraction, where the condensed parameters are directly calculated from the band-limited CIRs. More complex and computationally intensive high-resolution parameter extraction algorithms like SAGE [21], CLEAN [22] or RiMAX [23] could be used instead if a band-unlimited channel response is desired. σ_c^{CP} then remains a measure for the uncertainty due to random variations. Optionally, a multipath threshold could be applied to limit the instantaneous dynamic range of a channel response. In that case, $\epsilon_c^{\mathrm{TH,CP}}$ can be redefined as the bias between a thresholded and thresholdless band-unlimited channel, where the thresholded band-unlimited channel is introduced as band-unlimited equivalent

of the thresholded band-limited channel. The uncertainty analysis methodology proposed in Section II-D is applicable to both classical and high-resolution parameter extraction.

D. OVERVIEW OF UNCERTAINTY ANALYSIS METHODOLOGY

We propose a methodology to estimate uncertainty metrics for condensed parameters of individual measured channels. An overview of this methodology is depicted in Fig. 6. Band-unlimited reference channels are created in stage A. These channels should approximate the underlying band-unlimited response of the corresponding measured channels as accurately as possible. Therefore, a set of measured channels is utilized to create a reference channel for each individual (measured and band-limited) channel in the set. The utilization of a set of channels instead of an individual channel improves this approximation. In stage B, the unimpaired receive (Rx) signals are derived and the effects of the bandwidth limitation of the channel sounder are added. The hardware impairments are added to the Rx signals in stage C. In stage D, the processing (including processing impairments and either classical or high-resolution parameter extraction) is applied and the uncertainty metrics are calculated. The uncertainty analysis methodology is explained in more detail below.

1) STAGE A: CREATE REFERENCE CHANNELS

The goal in stage A is to create N_c band-unlimited reference channels. For this, the band-unlimited response must be determined from the band-limited responses of real, measured channels. The basis of the reference channel creation is a multidimensional MPC extraction technique, which exploits all available dimensions (e.g., delay, Doppler and angular) of the CIR to extract MPCs and their characteristics. One problem that needs to be solved for this is the fact that interfering MPCs cannot be distinguished in a band-limited CIR. Otherwise, it can lead to an underestimation of σ_c^{CP} (a single MPC namely results in less variations between snapshots than an interfering pair) and ϵ_c^{CP} (the magnitude of the single detected MPC is typically not equal to the sum of the magnitudes of the two interfering MPCs). Therefore, an additional step is applied to identify and include MPC interference. In this step, variations between snapshots within a measurement (e.g., the variations between snapshots in Fig. 4) and variations between different measurements within a set (e.g., the ripple effect in Fig. 3) are exploited as is explained in more detail in Section III-A. The result of stage A is a set of N_c band-unlimited reference channels.

A main difference between this reference channel creation method and conventional high-resolution parameter extraction algorithms is the ability to use information from multiple measurements within a set to detect interfering MPCs. This is important for accurate estimation of the uncertainty metrics. For example, the interference effect in Fig. 3 is difficult to detect for conventional high-resolution parameter extraction algorithms due to very small relative differences in delay,
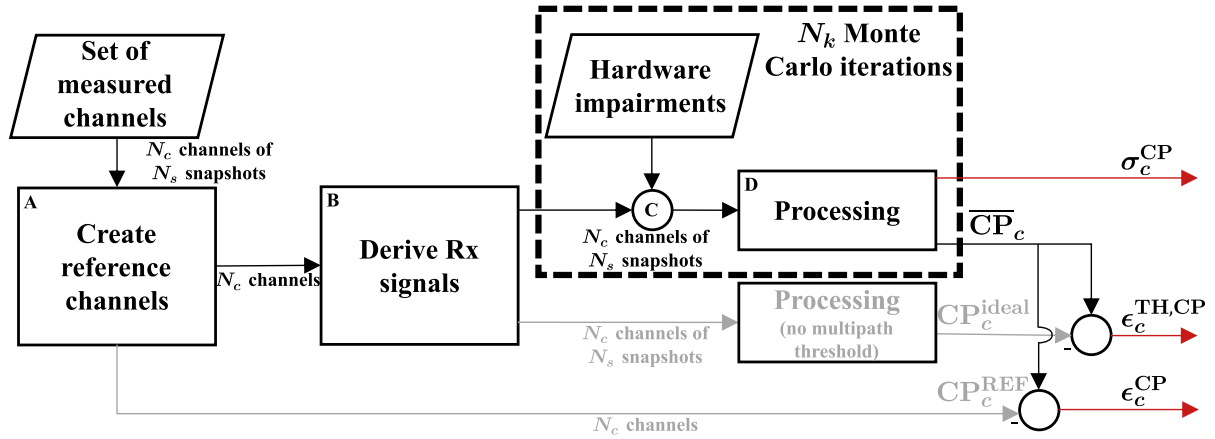
FIGURE 6. Overview of proposed uncertainty analysis methodology. This methodology enables the estimation of uncertainty metrics for condensed parameters of individual measured channels.

Doppler frequency, angle-of-departure and angle-of-arrival of the direct and ground-reflected MPCs. However, one could alternatively use a high-resolution parameter extraction algorithm when confident that it can sufficiently detect interfering MPCs in the given measurement data.

2) STAGE B: DERIVE RX SIGNALS

In stage B, the unimpaired received signals are derived for all reference channels. An Rx signal consists of N_p superimposed copies of the band-limited Tx signal, where N_p is the number of MPCs. Each copy is affected by the characteristics of the corresponding MPC.

A channel measurement often consists of multiple snapshots. For example, the PDP is derived from multiple snapshots in (1). The (unimpaired) Rx signals of these snapshots can differ due to channel dynamics. A non-zero Doppler frequency of an MPC in a dynamic measurement namely results in different delays and phases of this MPC in different snapshots. In addition, the use of antenna arrays for angular measurements introduces differences between snapshots. The delay and phase of an MPC can namely differ between snapshots taken at different antenna elements. To account for these effects, an Rx signal is derived for each of the N_s snapshots of a reference channel.

3) STAGE C: ADDITION OF HARDWARE IMPAIRMENTS

In stage C, hardware impairments are applied to the Rx signals. Some hardware impairments like thermal noise have a random nature. In addition, correlations between impairments and non-linearities in processing are expected. Therefore, a Monte Carlo simulation of N_k iterations is used for stages C and D. The Monte Carlo simulation also eases the addition of other hardware impairments and allows for any processing algorithm to be used.

4) STAGE D: PROCESSING

The Rx signals, including hardware impairments, are processed in stage D. The classical or high-resolution parameter extraction algorithm of the channel sounder is applied and the

processing impairments are included here. This results in N_k sets of condensed parameters for each reference channel. A Normal distribution is fit to the N_k observations of each condensed parameter. From these distributions, the mean value, $\overline{CP}_c$, and standard deviation, σ_c^{CP}, are extracted for each condensed parameter CP of each reference channel c. σ_c^{CP} is the standard uncertainty that is defined in Section II-C. $\overline{CP}_c$ is the average response of a condensed parameter of reference channel c. This parameter is needed for the estimation of uncertainty metrics $\epsilon_c^{TH,CP}$ and ϵ_c^{CP}.

The estimation of $\epsilon_c^{TH,CP}$ requires an observation of the condensed parameters without application of a multipath threshold. A parallel processing chain, which processes the Rx signals without applying any impairments, is introduced for this purpose. A threshold is still required in the calculation of the resulting condensed parameters, CP_c^{ideal}, to account for the finite dynamic range of the sounding signal. However, the dynamic range of the sounding signal (e.g., 72 dB for the TU/e channel sounder) is typically much larger than conventional multipath thresholds of 20 dB or 30 dB [24]. Therefore, the threshold can be chosen low enough to approximate the response without a threshold. $\epsilon_c^{TH,CP}$ can then be calculated for each condensed parameter of each reference channel as

$$\epsilon_c^{TH,CP} = \overline{CP}_c - CP_c^{ideal}. \quad (2)$$

Finally, the bias ϵ_c^{CP} is estimated. The band-unlimited response of the condensed parameters, CP_c^{REF}, is calculated directly from the MPCs in the reference channels. ϵ_c^{CP} is then calculated as

$$\epsilon_c^{CP} = \overline{CP}_c - CP_c^{REF}. \quad (3)$$

III. IMPLEMENTATION EXAMPLE OF UNCERTAINTY ANALYSIS METHODOLOGY USING TU/E CHANNEL SOUNDER

The proposed uncertainty analysis methodology can be applied to static and dynamic channel sounding measurements of any wideband channel sounder. In this section, the
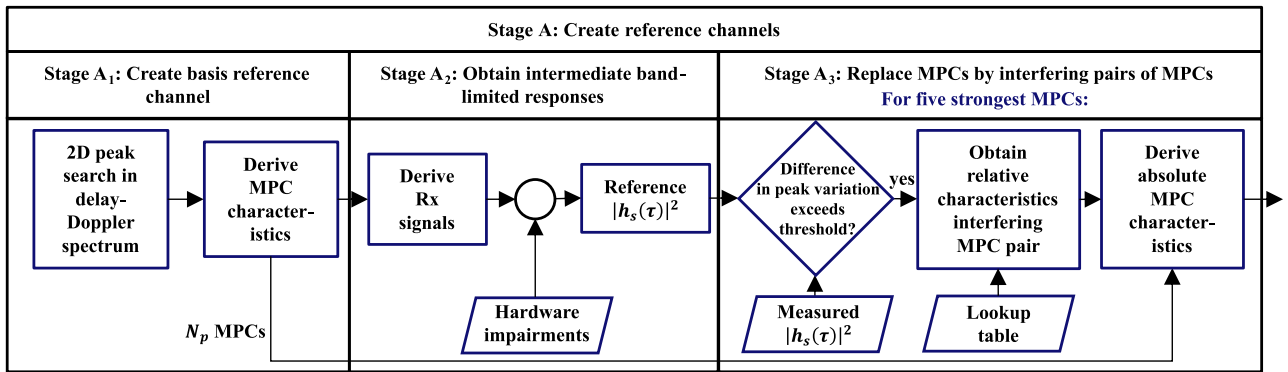
FIGURE 7. Block diagram showing the reference channel creation in stage A for the uncertainty analysis implementation of the TU/e channel sounder. The basis of the reference channel is created in stage A_1 by a 2D peak search in the delay-Doppler spectrum. A pair of interfering MPCs, which could not be distinguished in the 2D peak search, replaces the single detected MPC in stage A_3. Stage A_2 derives the band-limited responses that are needed in stage A_3.
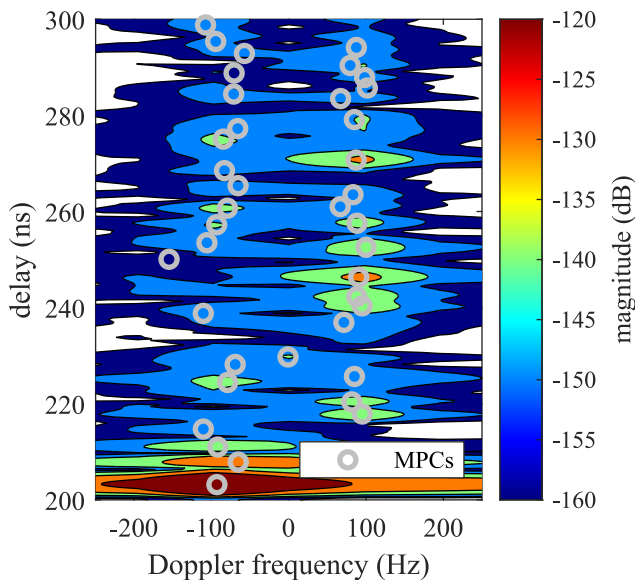

FIGURE 8. Example of estimated MPCs detected via a 2D peak search in delay-Doppler spectrum.

proposed uncertainty analysis methodology is implemented for dynamic channel sounding measurements of the TU/e channel sounder. This illustrates how the general uncertainty analysis methodology can be applied to a specific channel sounder. This implementation is also used for the verification in Section IV and to obtain exemplary results in Section V.

The TU/e channel sounder is introduced in [10] and its implementation is described in more detail in Appendix. This channel sounder derives the condensed parameters path loss, delay spread and Doppler spread. It uses 50 snapshots per measurement and a 20 dB multipath threshold in its processing. The uncertainty analysis methodology is implemented for its single-input-single-output (SISO) response.

A. STAGE A: CREATE REFERENCE CHANNELS

The delay and Doppler dimensions of the TU/e channel sounder can be leveraged for its reference channel creation. In addition, sets of measurements as well as its 50 snapshots can be exploited to add interfering MPC pairs. Fig. 7 depicts a flowchart of the reference channel creation in stage A for the TU/e channel sounder implementation. A basis for the reference channel is created in stage A_1 using a 2D peak search in the delay-Doppler spectrum. Variations between snapshots within a measurement and variations between measurements within a set are exploited in stage A_3 to replace single MPCs into interfering MPC pairs when interference is detected. In stage A_2, intermediate band-limited responses are calculated to enable the detection of interference in stage A_3. This implementation leads to the creation of reference channels, which are representative of the measured channels. The sub-stages of the reference channel creation are explained in more detail below.

1) STAGE A_1: CREATION OF BASIS REFERENCE CHANNEL

For the TU/e channel sounder, the basis of a band-unlimited reference channel is created from a band-limited measured channel in stage A_1. MPCs are detected via a 2D peak search in the delay-Doppler spectrum. An example of this is depicted in Fig. 8. MPCs can be distinguished within the Fourier limits of the delay and Doppler dimensions. Each MPC is defined by its magnitude a_p, delay τ_p, phase ϕ_p and Doppler frequency v_p. The required threshold to exclude noise peaks is lower than the noise floor of $p(\tau)$. This is due to the coherent averaging effect of noise in the delay-Doppler spectrum calculation and improves the ability to reconstruct weak MPCs. An additional 10 dB threshold is applied to the strongest peak at each delay index to prevent sidelobes in the Doppler dimension to be detected as MPCs. The output of this stage is a set of MPCs, which form the basis of the band-unlimited reference channel.
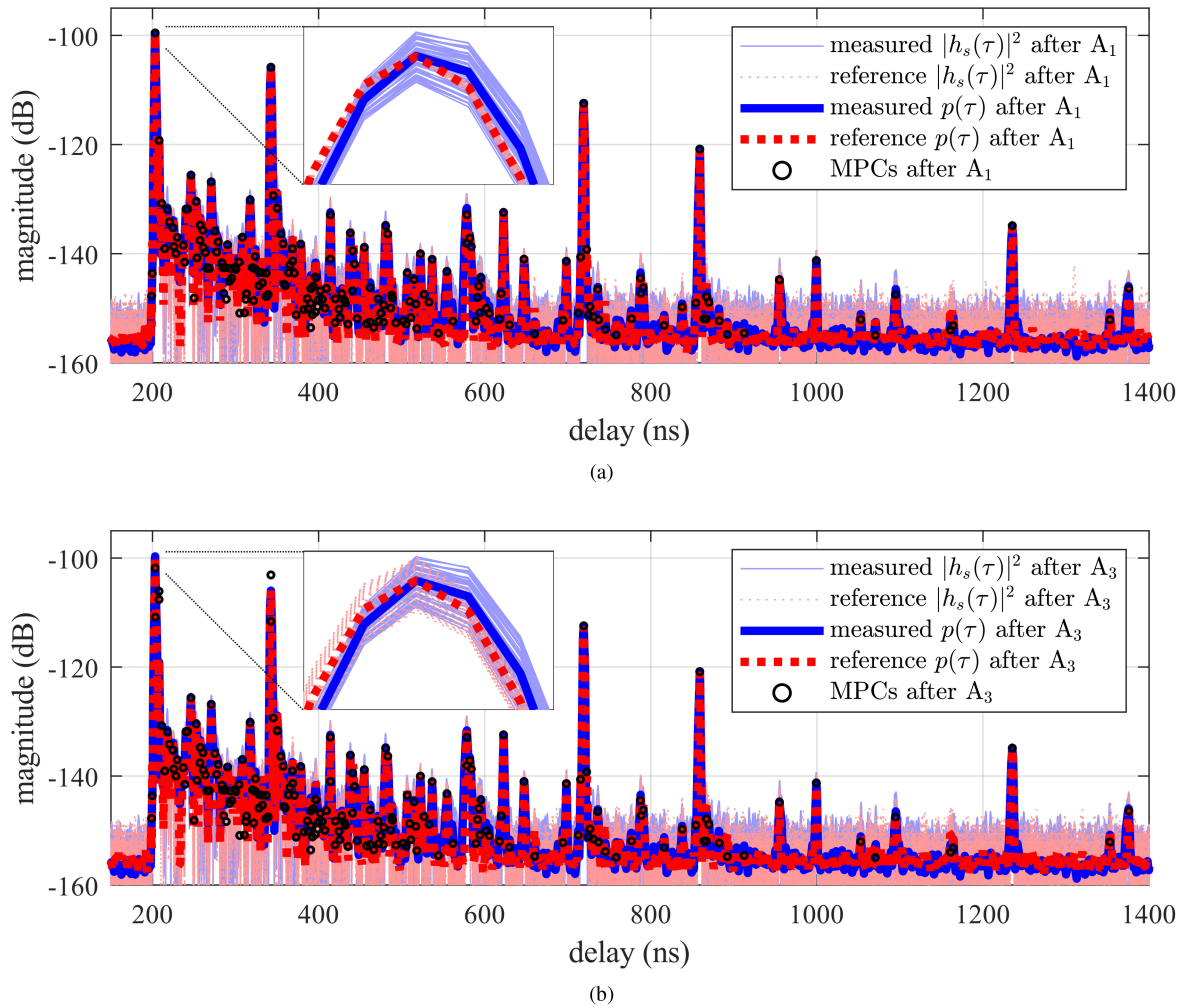
FIGURE 9. Example of the band-limited responses of a created reference channel, which is depicted by its MPCs. The average PDP and PDPs of individual snapshots are compared to the equivalent parameters of the corresponding measured channel for (a) the basis reference channel at the output of stage A_1 and (b) the final reference channel at the output of stage A_3. The average channel behavior is captured by the MPCs created in stage A_1. Stage A_3 is necessary to properly model variations between the PDPs of individual snapshots, which are caused by interference between MPCs.

2) STAGE A_2: OBTAIN INTERMEDIATE BAND-LIMITED RESPONSES

The basis of the reference channel, which is created in stage A_1, can be compared to the corresponding measured channel to assess how well it represents it. The band-limited response of the reference channel is required for this and is obtained in stage A_2. In this stage, the Rx signals are derived, hardware impairments are applied and the PDPs of individual snapshots are obtained. These steps are equivalent to the steps in stage B, C and the first step in stage D, which are explained in more detail in Sections III-A–III-D.

An example of a comparison between a measured channel and the corresponding reference channel after stage A_1 is depicted in Fig. 9(a). $p(\tau)$ shows a good match between the reference and measured channel, which means that the average behavior of the channel is reconstructed well in stage A_1. However, variations between some peaks of the individual $|h_s(\tau)|^2$ are not reconstructed well in stage A_1,

because this stage detects interfering MPCs as a single MPC. This is corrected for in stage A_3.

3) STAGE A_3: REPLACE MPCS BY INTERFERING PAIRS OF MPCS

Stage A_3 replaces single MPCs by interfering pairs of MPCs when interference is detected. The detection is implemented as a quantitative equivalent of the comparison between the variation in measured and reference $|h_s(\tau)|^2$ peaks in Fig. 9(a). If the difference between these variations exceeds a threshold, then it is estimated that this variation is not caused by the earlier included impairments. The single MPC is then replaced by an interfering pair with relative characteristics, which result in a similar variation as in the measured $|h_s(\tau)|^2$. These relative characteristics are obtained from a lookup table, which is generated by leveraging knowledge about all measured channels in the set. Finally, the absolute characteristics of the interfering MPCs are determined using

TABLE 2. Search space limits and step size for lookup table of LOS measurement set with interference between direct MPC and ground-reflected MPC.

Parameter	Min	Step	Max
Δa^2 (dB)	-10	0.5	0
$\Delta \phi$ (rad)	0	0.2π	π
$\Delta \nu$ (Hz)	1	1	10

the characteristics of the originally detected single MPC and the obtained relative characteristics.

Stage A_3 is only applied to the five strongest MPCs in a reference channel in order to limit computation time. More MPCs could be included if computation time is not a limitation. However, the benefit of this will typically be limited, because variations in weaker MPCs will have a smaller impact on the uncertainty metrics than variations in the (five) strongest MPCs. In addition, large variations in weak MPCs are typically caused by noise.

The variation in the magnitude of a peak over all N_s snapshots of $|h_s(\tau)|^2$ is approximated by a Normal distribution for both the reference and corresponding measured peak. The single MPC is replaced by an interfering pair if the standard deviation of the reference peak exceeds the standard deviation of the measured peak by an empirically estimated factor of 0.03 dB. This factor provides a safety margin between slight differences in the random impaired channel realizations and larger differences due to interference.

Each MPC has four degrees of freedom. Thus, there is a large number of possible MPC combinations that could cause a certain peak variation. Most of these variations can be reconstructed by two interfering MPCs with equal delay. Therefore, the delays of the interfering pair are chosen equal to the delay of the original MPC. The set of possible combinations of interfering MPCs can be further limited if the dominant interference mechanism can be qualitatively estimated for the given measurement set. For example, the presence of the ground-reflected MPC in Fig. 2 can be predicted from the ripple in Fig. 3. The example in Fig. 9(a) is taken from a LOS measurement with a similar interference between a direct MPC and a ground-reflected MPC. The range of the possible relative differences in magnitude of these MPCs can be estimated from the reflection coefficient of the floor. In addition, the relative difference between the Doppler frequencies of these MPCs is limited for large Tx-Rx distances. Using these observations, we can limit the range of possible relative MPC characteristics to the limits given in Table 2, where Δa^2, $\Delta \phi$, $\Delta \nu$ are the relative power, phase and Doppler frequency between the two interfering MPCs, respectively.

A lookup table for the search space in Table 2 is generated prior to the uncertainty analysis. The lookup table lists two parameters for each combination of the relative MPC characteristics from Table 2:

1) The peak-to-peak power variation between the peaks of all N_s realizations of $|h_s(\tau)|^2$. In case of interference between two MPCs, the $|h_s(\tau)|^2$ peak variation can be approximated by a uniform distribution. The entry in the lookup table with a peak-to-peak variation that is closest to the peak-to-peak variation in the measured $|h_s(\tau)|^2$ is selected as best estimate.

2) The power offset of the strongest MPC of the interfering pair with respect to the original MPC.

The characteristics of the strongest MPC of the interfering pair are identical to the characteristics of the original MPC, except for the power offset correction. The other MPC has the same delay as the strongest MPC. Its magnitude, phase and Doppler frequency are obtained by adding the relative characteristics Δa^2, $\Delta \phi$, $\Delta \nu$ from the chosen entry of the lookup table to the corresponding characteristics of the strongest MPC.

Fig. 9(b) compares the band-limited response of a reference channel at the output of stage A_3 to the response of the corresponding measured channel. The single MPC at the highlighted MPC peak position is replaced by an interfering pair of MPCs, which correctly models the power variation in the reference $|h_s(\tau)|^2$ peak. This variation can be reconstructed well for any channel, which improves the estimation accuracy of σ_c^{CP}. It is verified in Section IV-C that the resulting ϵ_c^{CP} is accurate for a set of channels when the search space of the interfering pair is refined. However, ϵ_c^{CP} cannot be evaluated if the search space for the interference is not refined, because the search space will then have local optima with similar peak variations for largely varying MPC characteristics.

B. STAGE B: DERIVE RX SIGNALS

In stage B, the Rx signal is derived for each snapshot. The Rx signal contains a delayed, phase-shifted and scaled copy of the transmitted maximum-length sequence for each MPC in the reference channel. For the TU/e channel sounder, the baseband equivalent of the unimpaired Rx signal of snapshot s can be calculated as

$$r_s = \sum_p \mathcal{F}^{-1}\left[\mathcal{F}[MLS] \circ e^{-j2\pi\left(\tau_p + \Delta\tau_p^s\right)\circ\xi} \right]$$
$$\circ e^{j\left(\phi_p - 2\pi f_{RF}\Delta\tau_p^s\right)} a_p, \qquad (4)$$

where $\mathcal{F}$ and $\mathcal{F}^{-1}$ denote the discrete Fourier transform and inverse discrete Fourier transform, respectively, and $\circ$ denotes an element-wise multiplication. MLS is the sampled maximum-length sequence, ξ the frequency vector of the sampled sequence, f_{RF} the carrier frequency and

$$\Delta\tau_p^s = \frac{v_p}{f_{RF}}\left(\tau + \frac{1}{f_t}\left(s - \frac{N_s}{2} - 1\right)\right), \qquad (5)$$

where τ is the delay vector. $\Delta\tau_p^s$ is the relative delay of MPC p of snapshot s with respect to the middle snapshot of a measurement. The unimpaired Rx signals are obtained from their baseband equivalents after inverting the post-processing steps in Appendix.
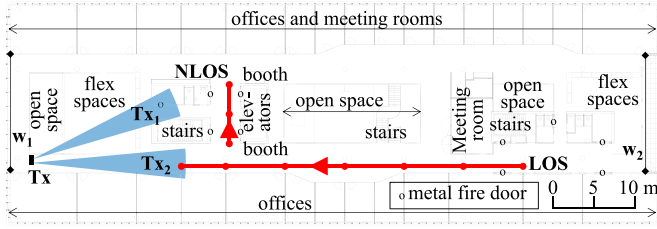
FIGURE 10. Measurement tracks for a LOS and NLOS set, where the Rx is moved at walking speed along the red lines. The LOS set only includes SISO channels from Tx_2, while the NLOS set includes SISO channels from both Tx_1 and Tx_2.

C. STAGE C: ADDITION OF HARDWARE IMPAIRMENTS
Hardware impairments of the channel sounder are added to the Rx signals in stage C. The focus in this paper is on uncertainty in dynamic channel measurements. Therefore, only hardware impairments that cause variations between snapshots within a measurement are included, which are thermal noise, quantization noise and jitter. Other (static and long-term varying) impairments could be added to improve the overall uncertainty estimation.

Thermal noise and jitter are estimated as Type A uncertainties and modeled as zero-mean Gaussian random variables with standard deviations σ_{TN} and σ_{JT}, respectively, and added to the unimpaired Rx signal samples. $\sigma_{TN} = 6.7$ mV is estimated via a terminated-Rx measurement, where the input of the Rx was terminated by a 50 Ohm load. $\sigma_{JT} = 0.26$ ps is estimated using the method described in [25], where σ_{JT} is the time-Allan deviation with an observation interval equal to the snapshot interval. Quantization noise is estimated as a type B uncertainty and included by quantizing the Rx signals (including thermal noise and jitter) using the amplitude levels of the digitizer.

D. STAGE D: PROCESSING
The obtained impaired Rx signals are post-processed in stage D using the steps and equations described in Appendix to obtain the condensed parameters path loss, delay spread and Doppler spread. These steps are thus identical to the post-processing steps of the TU/e channel sounder. The uncertainty metrics σ_c^{CP}, $\epsilon_c^{TH,CP}$ and ϵ_c^{CP} are estimated using the general stage D steps, which are explained in Section II-D.

IV. VERIFICATION OF METHODOLOGY USING TU/E CHANNEL SOUNDER
The proposed uncertainty analysis methodology is verified with the TU/e channel sounder using a LOS measurement set. This set consists of $N_c = 100$ SISO channel measurements with $N_s = 50$ snapshots, which are taken along the LOS track depicted in Fig. 10. These measurements are taken from the campaign described in [10]. This set of measurements exhibits the two-ray interference as modeled in Section II-A and uses the search space limits in Table 2. $N_k = 100$ Monte Carlo iterations are used in the analysis.

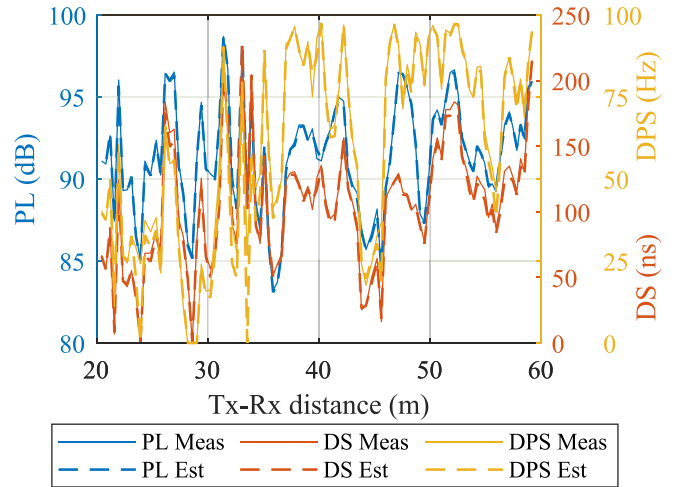Three aspects of the uncertainty analysis methodology are verified:

FIGURE 11. Comparison of estimated (Est) $\overline{CP}_c$ to the measured (Meas) condensed parameters of the corresponding channels in the LOS set. There is a very good agreement between the estimated and measured condensed parameters, showing that the created reference channels exhibit very similar average behavior as the corresponding measured channels.

1) The average responses of the condensed parameters of the reference channels should be similar to those of the measured channels. This gives confidence that the reference channels are representative of the corresponding measured channels.
2) The random variations in condensed parameters of reference channels should be similar to those of corresponding measured channels. This gives confidence that random impairments are well accounted for by the methodology.
3) Interference effects should be reconstructed well in the reference channels in order for the uncertainty metric ϵ_c^{CP} to be accurate.

The verification of these aspects is discussed in more detail below.

A. AVERAGE RESPONSE CONDENSED PARAMETERS
The average response of the condensed parameters is verified by comparing the estimated $\overline{CP}_c$ to the condensed parameters of the corresponding measured channels. This comparison is made in Fig. 11, which shows a very good agreement between the estimated and measured condensed parameters for all channels. The average behavior of the reference channels is thus representative of the average behavior of the measured channels using the proposed uncertainty analysis methodology.

B. RANDOM VARIATIONS IN CONDENSED PARAMETERS
Another important step is to verify that the random effects in the measurements are properly modeled in the uncertainty analysis. There is only one copy of each measurement. Therefore, the random variations in the path loss and delay spread of individual snapshots (calculated by bypassing the
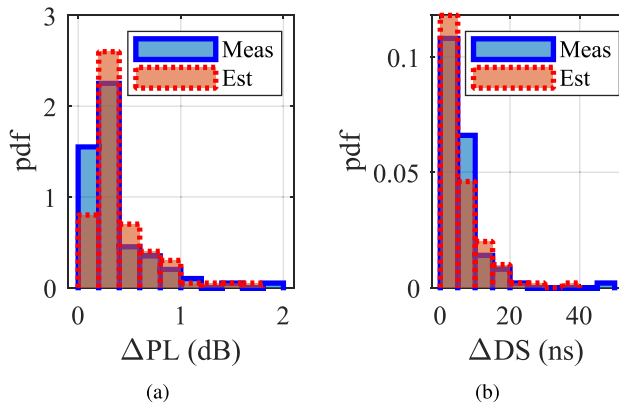
FIGURE 12. Maximum variation between snapshots of the measured (Meas) and estimated (Est) (a) path loss and (b) delay spread of the LOS set. This comparison shows that the modeled random effects result in a similar variation between snapshots for the estimated condensed parameters compared to the measured condensed parameters.
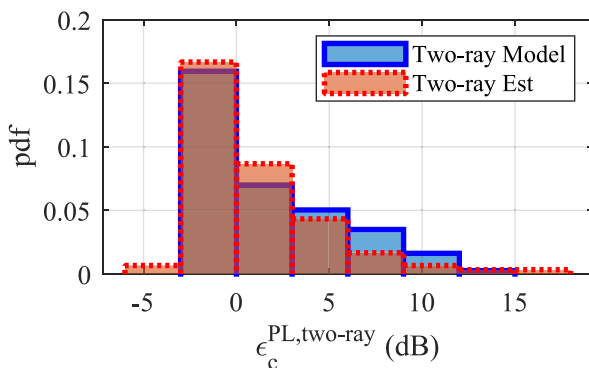

FIGURE 13. Comparison of the bias in path loss between the thresholded band-limited and thresholdless band-unlimited channel for the two-ray model and two-ray estimation (Est) of the LOS set. This comparison shows that the interference is properly reconstructed in the LOS set.

averaging step in (1)) are evaluated. A measure for the maximum variation between snapshots can be calculated for each channel as

$$\Delta\mathrm{CP} = \frac{1}{N_k}\sum_{k=1}^{N_k}\left(\max_{\forall s}(\mathrm{CP^s}) - \min_{\forall s}(\mathrm{CP^s})\right), \qquad (6)$$

where $\mathrm{CP^s}$ denotes the condensed parameter of an individual snapshot. N_k is set to 1 for the calculation of $\Delta\mathrm{CP}$ for the measured channels. The probability density functions (pdfs) of the resulting $\Delta\mathrm{PL}$ and $\Delta\mathrm{DS}$ of the estimated and measured responses for the LOS set are depicted in Fig. 12. There is a good agreement between the estimated and measured variations in condensed parameters, which gives confidence that the random effects are properly modeled in the uncertainty analysis.

C. RECONSTRUCTION OF INTERFERENCE
The estimation accuracy of ϵ_c^{CP} depends on how well interference between MPCs is reconstructed in the reference channels. The LOS set exhibits a similar two-ray

interference as the two-ray ground-reflection model in Fig. 2. Thus, the resulting biases in path loss due to interference can be compared. The LOS measurements also contain other MPCs than the direct and ground-reflected path. Therefore, the bias between the path loss of the thresholded band-limited and thresholdless band-unlimited channel is determined using only its PDP samples, which contain the direct and ground-reflected paths. The estimated and modeled biases, $\epsilon_c^{\mathrm{PL,two\text{-}ray}}$, are compared in Fig. 13. There is a good agreement between the estimated and modeled biases, which gives confidence that the proposed uncertainty analysis methodology accurately estimates ϵ_c^{CP}.

V. RESULTS OF METHODOLOGY FOR TU/E CHANNEL SOUNDER
In this section, uncertainty metrics for channel measurements of the TU/e channel sounder are presented and discussed. The purpose of this section is to illustrate how the uncertainty metrics of the presented methodology can be presented and interpreted. In addition, the uncertainties in the condensed parameters path loss, delay spread and Doppler spread of the TU/e channel sounder are discussed.

Uncertainty metrics are estimated for the LOS and non-line-of-sight (NLOS) measurement sets in Fig. 10. Both sets contain 100 channels. The search space limits in Table 2 are used in the analysis. This search space is not refined for the NLOS set. Therefore, the bias ϵ_c^{CP} is not estimated for this set. $N_k = 100$ is used for both sets. The pdfs of the uncertainty metrics of the channels in a set are presented next. These pdfs give an overview of the estimated uncertainty metrics within a set and enable comparisons of these metrics between different sets.

The pdfs of σ_c^{CP} for the condensed parameters path loss, delay spread and Doppler spread of the LOS and NLOS sets are depicted in Fig. 14. σ_c^{PL} is less than 0.005 dB and 0.02 dB for all channels in the LOS and NLOS set, respectively. The larger σ_c^{PL} in case of the NLOS set is due to the lower magnitudes of the NLOS MPCs, which increases the impact of thermal noise on the estimated path loss. The maximum expanded uncertainties for a 95% confidence interval are 0.01 dB and 0.04 dB for the LOS and NLOS set, respectively. This shows that these random variations have a negligible impact on the path loss. σ_c^{DS} and the corresponding expanded uncertainty for a 95% confidence interval are less than the 2.5 ns chip resolution. Similarly, σ_c^{DPS} and its expanded uncertainty are much less than the Doppler resolution of 97.7 Hz. The averaging factor of 50 in (1) is thus sufficient for the TU/e channel sounder to limit random variations due to impairments.

The pdfs of $\epsilon_c^{\mathrm{TH,CP}}$ are shown in Fig. 15. The LOS set shows a relatively small bias of up to 0.3 dB for most measurements. This is due to its dominant direct path, which is typically much stronger than the majority of other MPCs. A small subset of this set, which consists of measurements with a small Tx-Rx distance and destructive interference between the direct and ground-reflected MPCs, has a bias of
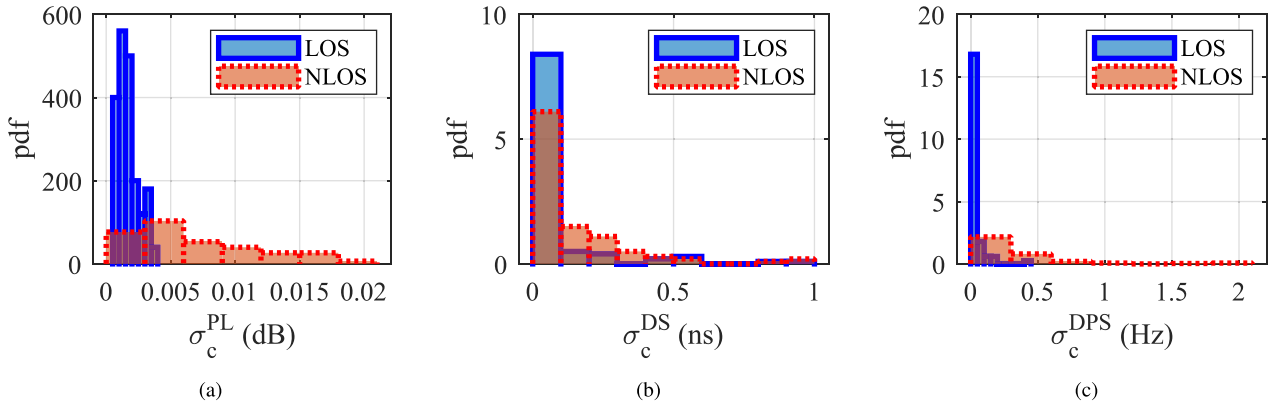
FIGURE 14. Distributions of σ_c^{CP} for the condensed parameters (a) path loss, (b) delay spread and (c) Doppler spread for all channels in the LOS and NLOS set. These uncertainties suggest that random variations due to impairments are limited for the TU/e channel sounder with $N_s = 50$.
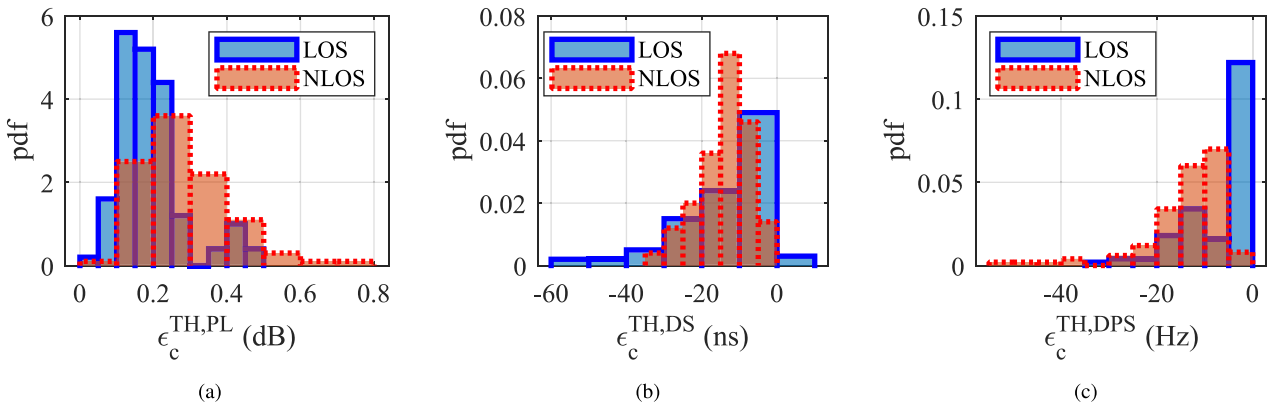

FIGURE 15. Distributions of $\epsilon_c^{TH,CP}$ for the condensed parameters (a) path loss, (b) delay spread and (c) Doppler spread for all channels in the LOS and NLOS set. The 20 dB multipath threshold of the TU/e channel sounder introduces a significant bias with respect to a thresholdless band-limited channel for the path loss and delay spread.
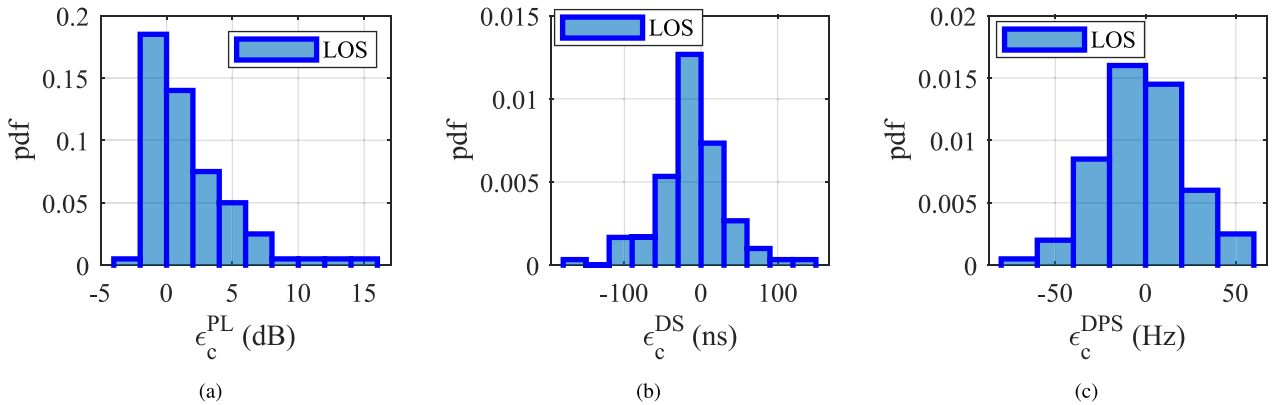

FIGURE 16. Distributions of ϵ_c^{CP} for the condensed parameters (a) path loss, (b) delay spread and (c) Doppler spread for all channels in the LOS set. These large biases are caused by interference between MPCs, which cannot be distinguished at the Fourier resolution.

0.4 to 0.5 dB. The NLOS set contains measurements with no dominant direct MPC and a richer multipath environment, which leads to a generally larger bias in path loss of up to 0.8 dB.

The 20 dB multipath threshold thus results in an overestimation of the path loss and an underestimation of the delay and Doppler spread. This bias could be reduced by increasing the threshold value. However, larger multipath thresholds increase the risk of including spurious MPCs. Moreover, large threshold values can limit the amount of measurements with sufficient instantaneous dynamic range for parameter extraction.

The pdfs of ϵ_c^{CP} are depicted in Fig. 16 for the LOS set. ϵ_c^{PL} is similar to the bias of the two-ray path loss in Fig. 13, because this bias is mainly determined by the interference between the direct and ground-reflected MPCs. It varies between -4 and 16 dB, which shows that the bandwidth limitation can introduce a large bias between the path loss of a band-limited and band-unlimited channel. ϵ_c^{DS} shows large biases over ± 100 ns. These large biases result from interference of the direct and ground-reflected MPCs in combination with the presence of MPCs at very large delays. This interference is also the cause of the spread in $\epsilon_c^{\mathrm{DPS}}$, where these biases are limited by the speed of the Rx.

Interference can thus introduce a very large bias between band-limited and band-unlimited condensed parameters. High-resolution parameter extraction is likely a better alternative than classical parameter extraction if band-unlimited responses are desired. However, information from multiple measurements might be required for such an algorithm to be able to correctly identify closely spaced interfering MPCs like a direct path and ground-reflection.

The results for the three uncertainty metrics highlight the big impact of the reference channel definition and selection on the uncertainty. These metrics allow evaluation of uncertainty for different reference channel definitions and also provide insight into the underlying causes.

VI. CONCLUSION

An uncertainty analysis methodology to quantify the uncertainties in condensed parameters of (dynamic) channel sounding measurements is presented. It is shown that uncertainties in condensed parameters can be highly channel dependent. Therefore, the proposed methodology derives reference channels from measured channels. Multiple measurements within a set and multiple snapshots within a measurement are exploited to improve the reference channel creation. Impairments are imposed on the reference channel and uncertainty metrics are estimated for the resulting condensed parameters. These metrics enable uncertainty estimation for various reference channel definitions.

The proposed uncertainty analysis methodology is implemented for the TU/e channel sounder. This implementation leverages aspects of this channel sounder to improve its reference channel creation. The methodology is verified with measurements of the TU/e channel sounder, which shows that the estimated parameters are in good agreement with equivalent measured and modeled parameters. Finally, the uncertainty metrics that result from the uncertainty analysis are presented for a LOS and NLOS set of measured channels. The estimated combined standard uncertainties are small, which shows that the random variation due to impairments are small. The biases introduced by the multipath threshold and interference are significant, which emphasizes the importance of a clear reference channel definition.

The presented methodology can also be used to improve the parameters and settings of a channel sounder. The impact of varying number of snapshots and snapshot intervals on
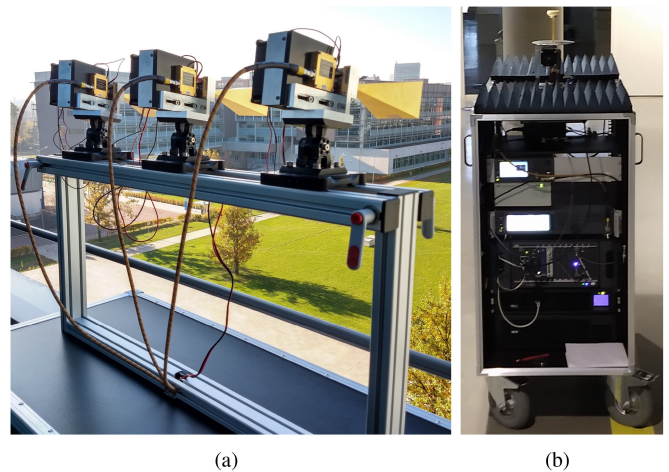

(a)   (b)

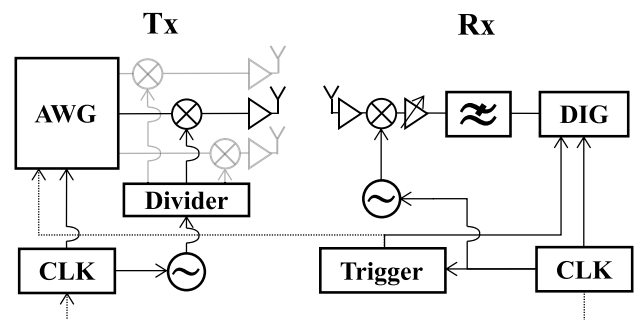**FIGURE 17.** Pictures of TU/e channel sounder (a) Tx and (b) Rx.

FIGURE 18. Block diagram of TU/e channel sounder. The uncertainty analysis is applied to the highlighted SISO response.

the uncertainty metrics could be investigated. In addition, the effect of different multipath threshold values could be analyzed.

APPENDIX
TU/E CHANNEL SOUNDER HARDWARE AND PROCESSING

The TU/e channel sounder is a 3x1 multiple-input-single-output (MISO) wideband correlation sounder and its Tx and Rx are depicted in Fig. 17. A block diagram of this channel sounder is illustrated in Fig. 18, where arbitrary waveform generator is abbreviated to AWG, rubidium clock to CLK and digitizer to DIG. This channel sounder is introduced in [10].

The main settings and parameters of the channel sounder are given in Table 3, and a timing and synchronization diagram is depicted in Fig. 19. A measurement is taken every 0.2 s. Every measurement consists of N_s snapshots recorded at trigger rate f_t, where the trigger rate is a power-of-two ratio of the 10 MHz rubidium clock frequency to achieve maximum long-term temporal stability. The sounding waveforms consist of maximum-length sequences of L chips at chip rate f_c, where the sequence period is $1/20^{\mathrm{th}}$ of the trigger period.
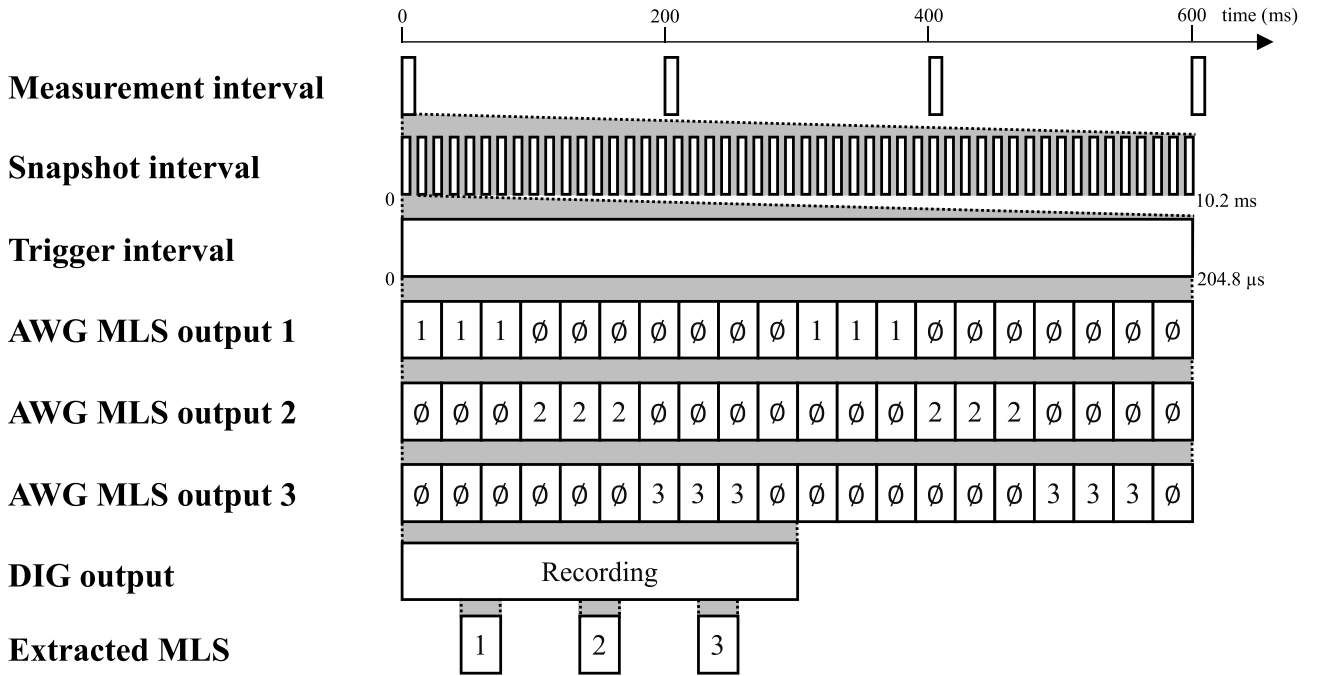
FIGURE 19. Channel sounder timing and synchronization diagram. A measurement is started every 0.2 s and consists of N_s snapshots. The arbitrary waveform generator (AWG) continuously transmits a repetitive sequence at each of its output channels. For every snapshot, one maximum-length sequence length is extracted from the digitizer (DIG) recording for each Tx channel.

The arbitrary waveform generator sequentially transmits three maximum-length sequences per Tx channel followed by one empty period to maintain synchronization. It is triggered once at the start of a measurement campaign and continuously transmits the same repetitive sequences at its output channels afterwards. The circular-shift property of the maximum-length sequence requires the arbitrary waveform generator to have transmitted one maximum-length sequence copy before the digitizer starts recording one maximum-length sequence length, and a third copy is needed for robustness against temporal drift. One maximum-length sequence length is extracted from the digitizer recording for each Tx channel. In post-processing, the sequence is down-converted to baseband, filtered and resampled to $8f_c$, which enables all further processing with exactly eight samples per chip.

For the uncertainty analysis, the path loss, delay spread and Doppler spread are derived from the single-input-single-output (SISO) response with vertically polarized antennas, where the transmit antenna has a 24 dBi gain and the receiving antenna a 3 dBi omnidirectional gain. The evaluation of the SISO channel is without loss of generality. For example, if the sequentially measured SISO channel responses are synthesized, then the uncertainty analysis methodology presented in Section II can be applied to each SISO channel and the path loss, delay spread and Doppler spread of the synthesized channels can be obtained by adjusting (7) and (13) below to include a summation over the SISO channels.

TABLE 3. TU/e channel sounder settings & parameters.

Parameter	Value
Carrier frequency f_{RF}	27 GHz
maximum-length sequence length L	4095 chips
Chip rate f_c	399.90234375 Mcps
Chip resolution	2.5 ns
Unambiguous range	3 km
# Snapshots per measurement N_s	50
Measurement interval	0.2 s
Trigger rate f_t	4.8828125 kHz
Doppler resolution	97.7 Hz
Maximum measurable Doppler frequency	2.4 kHz
Maximum velocity	96 km/h

The calibration method described in [13] is applied to the recorded signal to remove the system response from the measured channel response, using a back-to-back measurement between the Tx and Rx. A compensation for the antenna gains is then applied to obtain the CIR, $h_s(\tau)$ for every snapshot s. The average PDP can then be calculated as

$$p(\tau) = \frac{1}{N_s} \sum_{s=1}^{N_s} |h_s(\tau)|^2. \tag{7}$$

A multipath threshold 20 dB below the PDP peak value, as also used in [5], [7], [26], is applied to exclude potential spurious peaks that remain after calibration. All delay

indices, τ_{TH}, of a PDP above this threshold can then be defined as

$$\{\tau_{TH} \in \tau \land p(\tau_{TH}) > TH\}, \quad (8)$$

where TH is the threshold value. The path loss is calculated as

$$\text{PL} = -10 \log_{10}\left(\sum_{\tau_{TH}} p(\tau_{TH})\right) \quad (9)$$

and the rms delay spread is defined as

$$\text{DS} = \sqrt{\frac{\sum_{\tau_{TH}} \tau_{TH}^2 p(\tau_{TH})}{\sum_{\tau_{TH}} p(\tau_{TH})} - \left(\frac{\sum_{\tau_{TH}} \tau_{TH} p(\tau_{TH})}{\sum_{\tau_{TH}} p(\tau_{TH})}\right)^2} \quad (10)$$

[17]. The delay-Doppler spectrum can be calculated as

$$H(\tau, \nu) = \frac{1}{N_s} \sum_{s=1}^{N_s} h_s(\tau) e^{-\frac{j2\pi \nu(s-1)}{N_s}}, \quad (11)$$

where ν is the Doppler frequency [4]. The Doppler spread can be calculated in a similar way as the delay spread. Firstly, all samples in the Doppler spectrum that are above the threshold can be defined as

$$\left\{\left(\tau_{TH}^d, \nu_{TH}\right) \in (\tau, \nu) \land |H\left(\tau_{TH}^d, \nu_{TH}\right)|^2 > TH\right\}. \quad (12)$$

The Doppler power spectrum of the channel can then be calculated as

$$P(\nu_{TH}) = \sum_{\tau_{TH}^d} \left|H\left(\tau_{TH}^d, \nu_{TH}\right)\right|^2 \quad (13)$$

and the rms Doppler spread is calculated as

$$\text{DPS} = \sqrt{\frac{\sum_{\nu_{TH}} \nu_{TH}^2 P(\nu_{TH})}{\sum_{\nu_{TH}} P(\nu_{TH})} - \left(\frac{\sum_{\nu_{TH}} \nu_{TH} P(\nu_{TH})}{\sum_{\nu_{TH}} P(\nu_{TH})}\right)^2} \quad (14)$$

[17].

REFERENCES

[1] S. Rangan, T. S. Rappaport, and E. Erkip, "Millimeter-wave cellular wireless networks: Potentials and challenges," *Proc. IEEE*, vol. 102, no. 3, pp. 366–385, Mar. 2014.

[2] C. Gentile et al., "Methodology for benchmarking radio-frequency channel sounders through a system model," *IEEE Trans. Wireless Commun.*, vol. 19, no. 10, pp. 6504–6519, Oct. 2020.

[3] T. S. Rappaport, Y. Xing, G. R. MacCartney, A. F. Molisch, E. Mellios, and J. Zhang, "Overview of millimeter wave communications for fifth-generation (5G) wireless networks–with a focus on propagation models," *IEEE Trans. Antennas Propag.*, vol. 65, no. 12, pp. 6213–6230, Dec. 2017.

[4] P. B. Papazian, C. Gentile, K. A. Remley, J. Senic, and N. Golmie, "A radio channel sounder for mobile millimeter-wave communications: System implementation and measurement assessment," *IEEE Trans. Microw. Theory Techn.*, vol. 64, no. 9, pp. 2924–2932, Sep. 2016.

[5] G. R. MacCartney and T. S. Rappaport, "A flexible millimeter-wave channel sounder with absolute timing," *IEEE J. Sel. Areas Commun.*, vol. 35, no. 6, pp. 1402–1418, Jun. 2017.

[6] R. Müller et al., "Ultra-wideband channel sounder for measurements at 70 GHz," in *Proc. IEEE 81st Veh. Technol. Conf. (VTC Spring)*, 2015, pp. 1–5.

[7] S. Salous, S. M. Feeney, X. Raimundo, and A. A. Cheema, "Wideband MIMO channel sounder for radio measurements in the 60 GHz band," *IEEE Trans. Wireless Commun.*, vol. 15, no. 4, pp. 2825–2832, Apr. 2016.

[8] C. U. Bas et al., "Real-time millimeter-wave MIMO channel sounder for dynamic directional measurements," *IEEE Trans. Veh. Technol.*, vol. 68, no. 9, pp. 8775–8789, Sep. 2019.

[9] H. K. Kwon, M. D. Kim, and Y. J. Chong, "Implementation and performance evaluation of mmWave channel sounding system," in *Proc. IEEE Int. Symp. Antennas Propagat. USNC/URSI Nat. Radio Sci. Meeting*, 2015, pp. 1011–1012.

[10] R. Schulpen, L. A. Bronckers, A. B. Smolders, and U. Johannsen, "Impact of human blockage on dynamic indoor multipath channels at 27 GHz," *IEEE Trans. Antennas Propag.*, vol. 70, no. 9, pp. 8291–8303, Sep. 2022.

[11] "5G mmWave channel model alliance." Accessed: Oct. 1, 2022. [Online]. Available: https://sites.google.com/a/corneralliance.com/5g-mmwave-channel-model-alliance-wiki/home

[12] "IEEE P2982 recommended practice for Millimeter-wave channel sounder verification." Accessed: Oct. 1, 2022. [Online]. Available: https://sagroups.ieee.org/2982/

[13] P. B. Papazian et al., "Calibration of millimeter-wave channel sounders for super-resolution multipath component extraction," in *Proc. 10th Eur. Conf. Antennas Propag. (EuCAP)*, 2016, pp. 1–5.

[14] J. N. H. Dortmans, J. T. Quimby, K. A. Remley, D. F. Williams, J. Senic, and R. Sun, "Design of a portable verification artifact for millimeter-wave-frequency channel sounders," *IEEE Trans. Antennas Propag.*, vol. 67, no. 9, pp. 6149–6158, Sep. 2019.

[15] J. Quimby, D. G. Michelson, M. Bennai, K. Remley, J. Kast, and A. Weiss, "Interlaboratory millimeter-wave channel sounder verification," in *Proc. 13th Eur. Conf. Antennas Propag. (EuCAP)*, 2019, pp. 1–5.

[16] J. T. Quimby, D. F. Williams, K. A. Remley, D. Ribeiro, R. Sun, and J. Senic, "Millimeter-wave channel-sounder performance verification using vector network analyzer in a controlled RF channel," *IEEE Trans. Antennas Propag.*, vol. 69, no. 11, pp. 7867–7875, Nov. 2021.

[17] A. F. Molisch and M. Steinbauer, "Condensed parameters for characterizing wideband mobile radio channels," *Int. J. Wireless Inf. Netw.*, vol. 6, no. 3, pp. 133–154, 1999.

[18] *Evaluation of Measurement Data - Guide to the Expression of Uncertainty in Measurement*, Joint Committee Guides Metrol., Sèvres, France, JCGM 100:2008, 2008.

[19] "Effects of building materials and structures on radiowave propagation above about 100 MHz," ITU-R, Geneva, Switzerland, ITU-R P.2040–1, 2015.

[20] T. S. Rappaport, G. R. MacCartney, M. K. Samimi, and S. Sun, "Wideband millimeter-wave propagation measurements and channel models for future wireless communication system design," *IEEE Trans. Commun.*, vol. 63, no. 9, pp. 3029–3056, Sep. 2015.

[21] J. A. Fessler and A. O. Hero, "Space-alternating generalized expectation-maximization algorithm," *IEEE Trans. Signal Process.*, vol. 42, no. 10, pp. 2664–2677, Oct. 1994.

[22] J. A. Högbom, "Aperture synthesis with a non-regular distribution of interferometer baselines," *Astron. Astrophys. Suppl.*, vol. 15, p. 417, Jun. 1974.

[23] A. Richter, "Estimation of radio channel parameters: Models and algorithms," Ph.D. dissertation, Fakultät fur Elektrotechnik und Informationstechnik, Ilmenau Univ. Technol., Ilmenau, Germany, 2005.

[24] R. Schulpen, U. Johannsen, A. B. Smolders, and L. A. Bronckers, "Ambiguity in RMS delay spread of Millimeter-wave channel measurements," in *Proc. 17th Eur. Conf. Antennas Propagat. (EuCAP)*, 2023, pp. 1–5.

[25] R. Sun and P. B. Papazian, "Time stability of untethered electronic switched MIMO millimeter-wave channel sounders," *IEEE Access*, vol. 8, pp. 21052–21062, 2020.

[26] R. Müller et al., "Simultaneous multi-band channel sounding at mm-Wave frequencies," in *Proc. 10th Eur. Conf. Antennas Propag. (EuCAP)*, 2016, pp. 1–5.

ROBBERT SCHULPEN received the M.Sc. degree (cum laude) and the Ph.D. degree in electrical engineering from the Eindhoven University of Technology in 2017 and 2022, respectively, where he is currently a Postdoctoral Researcher of Electrical Engineering. His research interests include millimeter-wave metrology, millimeter-wave channel characterization and channel sounder design, calibration, and verification. He was awarded the Vederprijs 2022 for his research in millimeter-wave channel sounding.

A. BART SMOLDERS (Senior Member, IEEE) was born in Hilvarenbeek, The Netherlands, in 1965. He received the M.Sc. and Ph.D. degrees in electrical engineering from the Eindhoven University of Technology (TU/e) in 1989 and 1994, respectively. From 1989 to 1991, he worked as an IC Designer with FEL-TNO, The Hague. From 1994 to 1997, he was a Radar System Designer with Thales, The Netherlands. From 1997 to 2000, he was a Project Leader of Square Kilometer Array with the Netherlands Foundation for Research in Astronomy (ASTRON). From 2000 to 2010, he was with NXP (formerly Philips) Semiconductors, The Netherlands, responsible for the innovation in the RF business line. Since 2010, he has been a Full-Time Professor with the Electromagnetics Group, TU/e, with special interest in antenna systems and applications. Next to his research activities, he is the Dean of the Electrical Engineering Department, TU/e. He has published more than 150 papers. He currently leads several research projects in the area of integrated antenna systems operating at frequencies up to 150 GHz for several application domains, including 5G/6G wireless communications, radar sensors, and radio-astronomy. He is the Junior-Past Chairman of the IEEE Benelux Section and the Past-Chair of the Nederlands Radio- en Elektronica Genootschap. He is the Chairman of the Stichting Wetenschappelijke Activiteiten van het Nederlands URSI Committee and a member of the Advisory Board of ASTRON and PhotonDelta. For more information, see https://www.tue.nl/en/research/researchers/bart-smolders/.

ULF JOHANNSEN (Senior Member, IEEE) received the Dipl.-Ing. degree in communications engineering from the Hamburg University of Technology, Germany, in 2009, and the Ph.D. degree in electrical engineering from the Eindhoven University of Technology (TU/e), The Netherlands, in 2013.

From 2013 to 2016, he worked as a Senior Systems Engineer with ATLAS ELEKTRONIK GmbH, Bremen, Germany, where his role was a system designer and an engineering manager for autonomous underwater vehicle systems with sonar payloads. Since 2016, he has been with the Electromagnetics Group, Department of Electrical Engineering, TU/e, where he is currently an Associate Professor. He is the Head of the EM Antenna Systems Lab that focuses on innovative concepts and solutions for wireless applications from a system perspective. Since September 2023, he has also been serving as the Director of the Centre for Wireless Technology, TU/e, following a two-year part-time employment as a Senior Researcher with the Smart Frontend Group, Netherlands Institute for Radio Astronomy (ASTRON).

Dr. Johannsen is the Past Chair of the IEEE Benelux joint AP/MTT Chapter. Moreover, he serves on the advisory board of the Chip Integration Technology Centre, The Netherlands, and is an Independent Technology Advisor to ASTRON's Smart Frontend Group. He is an EuMA Member as well as an Associate Member of INCOSE.

L. A. (SANDER) BRONCKERS (Member, IEEE) received the M.Sc. degree (cum laude) in electrical engineering from the Eindhoven University of Technology (TU/e), The Netherlands, in 2015, and the Ph.D. degree (cum laude) in electrical engineering from the Electromagnetics Group, Tu/e in 2019, on design and measurement techniques for next-generation integrated antennas. In 2018, he was a Visiting Researcher with NIST, Boulder, Colorado, on antenna measurements in reverberation chambers. Since 2019, he has been an Assistant Professor of Metrology for Antennas and Wireless Systems with TU/e. In addition, he chairs the ultra high data rate track in the Centre for Wireless Technology Eindhoven. In 2020, he co-founded AntenneX BV, a spin-off focusing on high-frequency wireless characterization. His research interests include antenna (system) measurements in reverberation and hybrid chambers, channel sounding and emulation, and RF material characterization.